LAWRENCE
LIVERMORE
NATIONAL
LABORATORY

UCRL-JRNL-204047

The high-resolution architecture and structural dynamics of Bacillus spores

M. Plomp, T. J. Leighton, K. E. Wheeler, A. J. Malkin

May 10, 2004

Nature

The high-resolution architecture and structural dynamics of *Bacillus* spores

Marco Plomp[1], Terrance J. Leighton[2], Katherine E. Wheeler[2], Alexander J. Malkin[1]

[1]*BioSecurity & NanoSciences Laboratory, Lawrence Livermore National Laboratory, 7000 East Ave, Livermore, CA 94551*

[2]*Children's Hospital Oakland Research Institute, 5700 Martin Luther King Way, Oakland, CA 94609*

The capability to image single microbial cell surfaces at nanometer scale under native conditions would profoundly impact mechanistic and structural studies of pathogenesis, immunobiology, environmental resistance and biotransformation. We report here that advances in atomic force microscopy (AFM) have allowed us to directly visualize high-resolution native structures of bacterial endospores, including the exosporium and spore coats of four *Bacillus* species in air and water environments. The dimensions of individual *Bacillus atrophaeus* spores were found to decrease reversibly by 12% in response to a change in the environment from aqueous to aerial phase. Intraspecies spore size distribution analyses revealed that spore length could vary by a factor of 2 while the absolute deviation is 7 – 13% in length and 4 – 6 % in width. AFM analysis also demonstrated that the mechanisms of spore coat self-assembly are similar to those described for inorganic and macromolecular crystallization. These results establish AFM as a powerful new tool for the analysis of molecular architecture and variability as a function of spatial, temporal and developmental organizational scales.

Bacterial endospores are models for elucidating mechanisms of dormancy, chemical cueing of germination, and pathogenesis. Even though the complete genome sequences are available for *B. subtilis*, *B. cereus* and *B. anthracis*, the relationships

between spore architecture, spore coat topology and spore function are not understood. The spore coat[1] is a structural and reactive barrier that protects interior spore compartments including the DNA-containing core. In some spore-forming species, including *B. anthracis*, the etiological agent of anthrax, an exosporium structure overlays the spore coat.

Electron microscopic (EM) analysis of fungal and bacterial spores has demonstrated the presence of crystalline structures within the spore coat[2,3]**.** Conventional EM techniques require preparation and imaging of spores under non-physiological conditions. Sample preparation, which frequently involves fixation, staining, dehydration and embedding, can be damaging to the native structural integrity of biological specimens. An alternative high-resolution method to examine native spore ultrastructure is atomic force microscopy (AFM), which allows direct visualization of macromolecular assemblies *in vitro* at near-molecular resolution[4,5]**.** Using high-resolution AFM, we have recently demonstrated the ability to resolve native surface structures of several pathogens at ~ 20-30 Å resolution [6-9]. In the case of vaccinia virus [7], we have also shown that the internal virion structure can be revealed by chemical and enzymic nanodissection.

To study the topology and architecture of the outer spore integuments we visualized liquid and dried spore preparations from *B. thuringiensis*, *B. cereus*, *B. subtilis* and *B. atrophaeus* (Figs.1a,d,g). *B. thuringiensis* and *B. cereus* spores are enclosed in an exosporium (Fig. 1a,d), which is considerably larger than the underlying spore. The high-resolution structure of the exosporium of *B. cereus* spores (insert, Fig.1b) is composed of 12 –14 nm diameter subunits, which could represent exosporial proteins or their oligomers.

Removal of the *B. thuringiensis* (Fig.1a) and *B. cereus* (Fig.1d) exosporium by sonication revealed crystalline hexagonal honeycomb (Fig. 1c) and rodlet (Fig. 1e) outer spore coat structures respectively. The ~ 10 nm thick rodlet layer of *B. cereus* spores is formed by multiple randomly oriented domains, comprised of parallel subunits with a periodicity of ~ 8 nm. The size of the domains is typically 100 – 200 nm. Complete removal of the primary *B. cereus* rodlet layer by sonication revealed an underlying honeycomb structure (Fig. 1f) similar to the primary outer spore coat layer of *B. thuringiensis* (Fig. 1c). For both species, the lattice parameter for the honeycomb structure is ~ 9 nm, with ~5 – 6 nm holes/ pits (Fig.1c, 1f).

For *B. atrophaeus* (Fig.1g) and *B. subtilis* spores (data not shown here), the outer layer spore coat was composed of a crystalline rodlet layer with a periodicity of ~ 8 nm (Fig. 1h). In contrast to the multi-domain rodlet structure of the *B. cereus* spore coat (Fig.1e), generally only a single domain was found to be present on the outer coat of *B. atrophaeus* and *B. subtilis* spores, with the individual rodlets spanning the entire spore.

Similar rodlet and honeycomb crystalline structures to those seen in Figure 1, were observed in freeze-etching EM studies of several species of *Bacillus* spores [2,3] and AFM studies of fungal spores[10]. In the case of *B. thuringiensis*, spore coat rodlet structures were not observed in freeze-etching EM[2,3] or in the current AFM studies. However, as illustrated in Figure 1i, patches of adsorbed rodlets were observed on the substrate during AFM visualization of *B. thuringiensis* spores. Rodlet width and thickness (Fig. 1e) were similar to those observed for *B. atrophaeus* and *B. cereus* spore coat structures. Under different physiological conditions, it may be possible that extrasporal rodlets could self-assemble on the *B. thuringiensis* spore surface.

The striking differences in native rodlet motifs seen in *B. atrophaeus* (one major domain for each spore), *B. cereus* (a patchy multi-domain motif) and *B. thuringiensis* (extrasporal rodlets) appear to be a consequence of species-specific nucleation and crystallization mechanisms which regulate the assembly of the outer spore coat. The control of rodlet crystallization could depend on morphogenetic assembly factors, composition and concentration of the growth units, as well as on environmental factors, such as temperature, pH, metals and salts. In the case of *B. cereus* outer coat assembly, the surface free energy[11] for crystalline phase nucleation appears to be low enough to allow the nucleation of multiple rodlet domains resulting in cross-patched and layered assemblies. During the assembly of the outer coat of *B. atrophaeus* spores, the surface free energy may be considerably higher reducing nucleation to the point that only one major domain covering the entire spore surface is formed (Fig.2).

All *Bacillus* species investigated utilize very similar rodlet structures as spore coat building blocks. The mechanisms of self-assembly of spore coat structural layers appear to be very similar to those described for crystallization of inorganic single crystals[11] and macromolecular crystals grown for X-ray diffraction analysis[12,13]. Consequently, fundamental and applied concepts developed for the growth of inorganic and protein crystals can be successfully applied to study the assembly of the spore coat. The solution chemistry (i.e. concentration of assembly factors, spore coat proteins, small molecules, pH, temperature, etc.) during spore integument formation may control the macromolecular arrangement of rodlet motifs. Indeed, it has been reported that the addition of Na_2SO_3 during sporulation of *B. cereus* causes rodlet elongation and incomplete rodlet layer assembly[2]. Thus, spore coat structure architecture and topology may be genetically and environmentally determined. This suggests that AFM may be

useful for microbial forensic applications by reconstructing the environmental conditions that were present during spore formation.

Detailed knowledge of the physical response of spores to changes in their environment is paramount for understanding their structural dynamics, germination and inactivation by decontamination regimes. AFM allows a side-by-side comparison of high-resolution structures, morphology and individual spore dimensions in aqueous (Fig.3a) and aerial phases (Fig.3b). Air to water phase transitions does not affect the microscopic arrangement of the *B. atrophaeus* rodlet structure. However, upon drying, a significant deformation of the entire spore coat was observed (Fig.3b), resulting in the formation of 30 – 60 nm thick ridges extending along the entire spore surface with a number of shorter 5 – 15 nm thick wrinkles. Upon rehydration, a completely fitted rodlet layer, similar to one seen in Figure 3a, was re-established (data not shown). Dehydrated surface ridges (Fig. 3b) have been observed previously in EM[14] and AFM [15,16] studies of fungal and bacterial spores.

Formation of ridges upon dehydration was found to be accompanied by a pronounced decrease in spore size. The average width of 35 individual spores in air (65% relative humidity) was reduced to 88% of the size measured for aqueous phase spores (Fig. 3c). When the dried spores were rehydrated, they returned to 97% of their original size after 2 hrs in water, establishing the reversibility of the size transition. These individual spore measurements were confirmed by independent studies where *B. atrophaeus* spore width was measured from two independent sets of ~200 spores in water and air, respectively. The air-dried spore width was reduced 12% when compared to spores imaged in water. The observed decrease in the width of bacterial spores upon dehydration is apparently due to contraction of the spore core and/or cortex.

Size change experiments reported here confirm and extend recent experiments of two of the authors[17], where, using optical microscopy, a reversible size change of ~4% was measured for *B. thuringiensis* spores upon a change of relative humidity from 3% to >95%. Based on these experiments, it was further suggested[16] that the morphology of the spore coat could change upon swelling or shrinking of the spore. The direct visualization of individual spore environmental responses to dehydration/rehydration presented here clearly demonstrates that the spore coat itself does not shrink/expand but is flexible enough to compensate for the internal volume decrease of core/cortex compartments by surface folding and formation of ridges.

The studies reported here establish that the dormant spore is a dynamic physical structure. Spore swelling could play an important role during the emergence from the dormant state. Preliminary AFM studies suggest that additional alterations of spore dimensions accompany the initial stages of the germination process.

Size distributions from several large (~ 200) populations of spores were recorded. Both spore width and length were measured for hydrated and dried solution- and plate-grown *B. atrophaeus*, dried solution- and plate-grown *B. thuringiensis* and dried and solution-grown *B. subtilis* spores, respectively (Fig.4). The average values for spore width W_{av} and length L_{av} are given in **Table 1**, together with the absolute deviation *D*, defined as:

$$D_{x\,(x=W,L)} = \frac{1}{N}\sum_{i=1}^{N} \left| x_i - x_{av} \right| \qquad (1)$$

From these measurements, the deviation in width is 4 – 6% and for length is 7 – 13%.

By comparison, using EM images, the standard deviation (SD) for length and width of various *B. subtilis* spores was measured to be ~ 12%[18]. In these studies, the EM measurements are approximately comparable to a SD of 5 – 8% (length) and 8 – 17%

(width). The difference between the smallest and largest spores observed was a factor of ~ 1.5x in width, and approaches a factor of 2x for length. Even in the case of a single spore forming species and specific growth conditions, there is a wide distribution of smaller and larger size spores that could have significantly different dispersal, deposition and inhalation characteristics. The observed spore dimension variations within a single population are of particular importance to models that predict the environmental fate, transport and settling velocity of spores.

Spores of *B. thuringiensis* are substantially larger (~50% higher and ~20% longer) than *B. atrophaeus* and *B. subtilis* spores. The difference in average width and length between plate-grown and solution-grown spores of *B. atrophaeus* and *B. thuringiensis* suggest that environmental/physiological factors can have significant effects on spore dimensions.

We have demonstrated that AFM can address spatially explicit spore coat protein interactions and their structural consequences at near—molecular resolution. For the first time, the species-specific crystalline layers of the spore coat of *Bacillus* spores were observed at high-resolution in their natural environment, namely air and water. These results establish AFM as a powerful new tool capable of revealing bacterial spore structure and variability at nanometer-to-micrometer scales.

Methods

Spore Preparation and Purification

Spore preparations were produced using Schaeffer's sporulation medium as previously described [19]**.** Solid phase spore preparations were produced on agar plates containing Schaeffer's sporulation medium solidified with 1.5% agar (Difco). Spores were purified as previously described [20]. *Bacillus atrophaeus* (ATCC 9372) and *Bacillus thuringiensis israelensis* (ATCC 35646) were obtained from the American Type Culture Collection

(ATCC; Manassas, Virginia, USA). *Bacillus subtilis* 168 has been described previously [19].

Sonication was performed using a 20kHz 130W Vibra-cell VC 130 (Sonics & Materials, Newtown, CT) with a 3 mm probe. Spores were sonicated in an Eppendorf tube for 5 seconds, interspersed with 20-second cooling intervals (4ºC) to prevent excessive heating of the sample. The amplitude was increased from 0% to 30% and decreased to 0% for moderate sonication treatments, and increased to 50% for more intense sonication treatments (*B. cereus* spores). Spores were treated for 10 – 20 cycles of sonication.

Atomic Force Microscopy. For AFM observation, droplets of spore suspensions were deposited on mica, HOPG graphite, or plastic cover slips and incubated for 10 minutes, after which the sample substrate was carefully rinsed. For experiments in liquid, the resulting sample was imaged using an AFM fluid cell. For experiments in air, the sample was dried and imaged.

We used Digital Imaging (DI, Santa Barbara, CA) Nanoscope IIIa and IV atomic force microscopes operated in tapping mode. The AFM instruments were equipped with optical microscopes, which enabled us to track individual spores for imaging after a change of the environment. For imaging in air, DI and Olympus etched silicon tips with force constants of about 40 N/m and resonance frequencies of ~ 300 kHz were used. For imaging in water, DI and Olympus silicon nitride cantilevers (force constant 0.1 N/m) with either etched silicon or oxide-sharpened silicon nitride tips were used. Tapping amplitude, phase and height images were collected simultaneously. While height images were primarily used for quantitative measurements, amplitude and phase images were predominantly used for presentation.

For spore size determination, we measured both spore height and length. We assume height, just as spore *width* measured elsewhere using EM [18] and optical microscopy [17], to be identical to the *semi-minor axis* [17] and length to be identical to the *semi-major axis* [17]. Throughout the text we refer to height measurements as width measurements.

Dull or contaminated AFM tips can produce artefactual images of spores and other biological samples (unpublished data). Due to the limited sharpness of the AFM tip [21], artefacts can also arise when imaging relatively large particles such as spores. Size

measurements in the lateral AFM image plane can also have systematic errors, which differ from tip to tip. Therefore, each series of size measurements was performed with one single tip, to avoid systematic errors within a series. AFM height measurements do not suffer from this problem, and hence are more reproducible irrespective of tip geometry. Therefore, only height measurements were used in the case of monitoring the response in size dynamics of individual spores during changes from water to air environments.

References

1. Driks, A. Maximum shields: the assembly and function of the bacterial spore coat, *Trends in Microbiology* **10**, 251-254 (2002).

2. Aronson, A.I. & Fitz-James, P. Structure and morphogenesis of the bacterial spore coat, *Bacteriological Reviews* **40**, 360-402 (1976).

3. Wehrli, E., Scherrer, P. & Kubler, O. The crystalline layer in spores of *Bacillus cereus* and *Bacillus thuringiensis* studied by freeze-etching and high resolution electron microscopy. *Europ. J. Cell Biology* **20**, 283-289 (1980).

4. Binnig, G., Quate, C.F. & Gerber, C. Atomic force microscope, *Phys. Rev. Lett.* **56**, 930-933 (1986).

5. Bustamante, C., C. Rivetti, C. & Keller, D. Scanning force microscopy under aqueous solutions, *Curr. Opin. Str. Biol.* **7**, 709-716 (1997).

6. Plomp, M., Rice, M.K., Wagner, E.K., McPherson, A. & Malkin, A.J. Rapid visualization at high resolution of pathogens by atomic force microscopy: Structural studies of Herpes Simplex Virus-1. *Amer. J. Pathology* **160**, 1959-1966 (2002).

7. Malkin, A.J., McPherson, A. & Gershon, P.D. Structure of intracellular mature vaccinia virus visualized by *in situ* AFM. *J. Virol*., **77**, 6332-6340 (2003).

8. Malkin, A.J., Plomp, M. & McPherson, A. Unravelling of the architecture of human viruses by high-resolution atomic force microscopy. in *DNA Viruses: Methods and Protocols* (ed. P.M. Lieberman, P.M.), in press (The Humana Press Inc., 2004).

9. Malkin, A.J. & McPherson, A. Probing of crystal interfaces and the structures and dynamic properties of large macromolecular ensembles with *in situ* atomic force microscopy. in: *From solid-liquid interface to nanostructure engineering*. vol. 2.

Assembly in hybrid and biological systems. (eds. X.Y. Lin, X.Y. & DeYoreo, J.J.) 201-238 (Plenum/Kluwer Academic Publisher, 2004).

10. Dufrêne, Y.F., Boonaert, C.J.P., Gerin, P.A., Asther, M. & Rouxhet, P.G. Direct probing of the surface ultrastructure and molecular interactions of dormant and germinating spores of *Phanerochaete chrysosporium*, *J. Bacteriology* **181**, 5350-5354 (1999).

11. Chernov, A.A. *Modern Crystallography III. Crystal Growth*. (Springer-Verlag, Berlin, 1984).

12. McPherson, A. *Crystallization of Biological Macromolecules*. (Cold Spring Harbor Laboratory, 1999).

13. Vekilov, P.G., & Chernov, A.A. The Physics of Protein Crystallization, in *Solid State Physics* (eds. Ehrenreich, H. & Spaepen, F.) vol. **57**, 1-147 (Academic Press, New York, 2002).

14. Holt, S.C. & Leadbetter, E.R. Comparative ultrastructure of selected aerobic spore-forming bacteria: a freeze etching study. *Bacteriol. Rev*. **33**, 346-378 (1969).

15. Chada, V.G.R., Sanstad, E.A., Wang, R. & Driks, A. Morphogenesis of *Bacillus* spore surfaces, *J. Bacteriology* **185**, 6255-6261 (2003).

16. Driks, A. The dynamic spore, *PNAS* **100**, 3007-3009 (2003).

17. Westphal, A.J., Buford Price, P., Leighton, T.J. & Wheeler, K.E. Kinetics of size changes of individual *Bacillus thuringiensis* spores in response to changes in relative humidity, *PNAS* **100**, 3461-3466 (2003).

18. Leuschner G.K., Weaver, A.C. & Lillford, P.J. Rapid particle size distribution analysis of *Bacillus* spore suspensions, *Colloids and Surfaces B* **13**, 47-57 (1999).

19. Longchamp, P. & Leighton, T. Molecular recognition specificity of *Bacillus globigii* spore antibodies. *Lett. Appl. Microbiol*. **31**, 242-246 (2000).

20. Nicholson, W.L. & Setlow, P. Sporulation, germination, and outgrowth. in Molecular Biological Methods for *Bacillus* (eds. Harwood, C.R, & Cutting, S.M.) 391-450 (John Wiley & Sons, Chichester, West Sussex, UK 1990).

21. Velegol. S.B., Pardi, S., Li, X., Velegol, D., & Logan, B.E.AFM Imaging artefacts due to bacterial cell height and AFM tip geometry, *Langmuir* **19**, 851-857 (2003).

22. Chernov, A.A., Rashkovich, L.N., Yaminski, I.V., & Gvozdev, N.V. Kink kinetics, exchange fluxes, 1D ‘nucleation” and adsorption on the (010) face of orthorhombic

lysozyme crystals, *J. Physics-Condensed Matter*, **11**, 9969-9984 (1999).

Acknowledgements. We thank A. McPherson for the use of the scanning probe microscope facilities in his laboratory at the University of California, Irvine, and S. Velsko and J.J. DeYoreo for helpful discussions and encouragement, M.Pitesky for providing samples for initial experiments. This work was performed under the auspices of the U.S. Department of the Energy by the University of California, Lawrence Livermore National Laboratory under Contract W-7405-Eng-48 and with support from DARPA.

Competing interests statement. The authors declare that they have no competing financial interests.

Correspondence and requests for materials should be addressed to A.J.M. (e-mail: malkin1@llnl.gov).

Figure Legends

Figure 1. The spore coats of *B. thuringiensis* (a-c), *B. cereus* (d-f) and *B. atrophaeus* (g,h) consist of crystalline layers of honeycomb and rodlet structures. *B. thuringiensis* (a) and *B. cereus* (d) spores are surrounded by an exosporium (E), which 'deflates' and adheres to the substrate when spores are dehydrated. The exosporium (b) is 25 – 40 nm thick and has a ~3 nm thick and 20 – 30 nm wide footstep (F) with numerous thin (~1 nm) and short (50 – 60 nm) hair-like appendages (A2) attached to it. Additionally, there are typically 4 – 8 tubular appendages (A1) attached to the exosporium with a diameter and a length in the range of 3 – 12 nm and 300 – 1200 nm respectively. Underneath the exosporium, a honeycomb crystalline layer defines the outer surface of *B. thuringiensis* spores (c). This honeycomb layer is formed by domains with randomly oriented crystalline orientations, which are separated by linear defects. In panels (e) and (h) the crystalline rodlet structures of *B. cereus* and *B. atrophaeus* spore coats are shown. In *B. cereus* spores, underneath the rodlet layer there is a layer of crystalline honeycomb structure (f). While *B. thuringiensis* spore coats do not contain rodlets, they *can* be seen adsorbed on the substrate (i). Scale bar, 500 nm in (a,d,g); 50 nm in (b,c,e,f,h,I).

Figure 2. Crystallization of the rodlet layer on *B. atrophaeus* spore by a one-dimensional (1D) nucleation mechanism [22]. Once a nucleus is formed, it expands both by tangential growth of individual rodlets, with velocity V_t, and laterally by 1D nucleation of new rodlets with velocity of V_n. (a). If V_t is much larger than V_n, one single rodlet will grow rapidly and eventually inhibit itself, thereby prohibiting the formation of an organized, closed-packed layer (b). Similarly, if the 1D nucleation rate

V_n is much larger than V_t, this will result in multiple rings of short rodlets surrounding the spore, which were not observed experimentally. Hence, based on the observed rodlet spore structure, the two growth vectors for the major domain of spores of *B. atrophaeus* (Fig.1h) and patches of the *B. cereus* spore rodlet layer (Fig. 1e) must have similar growth rates.

Figure 3. The effects of changing the *B. atrophaeus* spore environment from aqueous to dehydrated states. (a) Phase image and height image (inset) detail of a *B. atrophaeus* spore in water, showing several shallow wrinkles. (b) The same spore after drying, showing many adsorbed stray rodlets, and a 60 nm high ridge (indicated with R). (c) Width change of 35 individual *B. atrophaeus* spores. Depicted is the individual measured spore width for a set of dehydrated (24 hrs) (diamonds, dashed trendline) and rehydrated (2 hours) spores (triangles, dotted trend line), as a function of the spore size of the originally hydrated spore. For ease of comparison, the original hydrated spore width is (redundantly) depicted as circles, which by definition lie on the solid $y=x$ line. Thus, the data points for one individual spore, depicted with the same color, are all on the same vertical line. On average, spore size is reduced to 88% for dried spores, and returns to 97% of the original width for rehydrated spores (see text). Scale bar, 200 nm.

Figure 4. Distribution of spore width (a) and length (b) for plate-grown (pg) and solution-grown (sg) *B. atrophaeus* and *B. thuringiensis* spores, and solution-grown *B. subtilis* spores. Statistics for these distributions are given in table 1.

Table 1. Average width, length and absolute deviations for several spore populations

	# spores	W_{av} [nm]	D_W [nm]	D_W [%]	L_{av} [μm]	D_L [μm]	D_L [%]
B. atrophaeus sg dried	264	626	27	4.2%	1.79	0.19	10%
B. atrophaeus pg dried	220	647	28	4.3%	1.68	0.13	7.8%
B. subtilis sg dried	202	713	32	4.5%	1.85	0.12	6.6%
B. thuringiensis sg dried	46	872	47	5.4%	2.00	0.16	7.8%
B. thuringiensis pg dried	153	937	49	5.3%	2.17	0.18	8.3%

sg = solution-grown, pg = plate-grown (pg), W,L_{av}. =average width resp. length, $D_{W,L}$ = absolute deviation in width resp. length

Fig. 1
Malkin

a	b	c
d	e	f
g	h	i

scalebars:

500 nm

500 nm

500 nm

50 nm

50 nm

50 nm

50 nm

50 nm

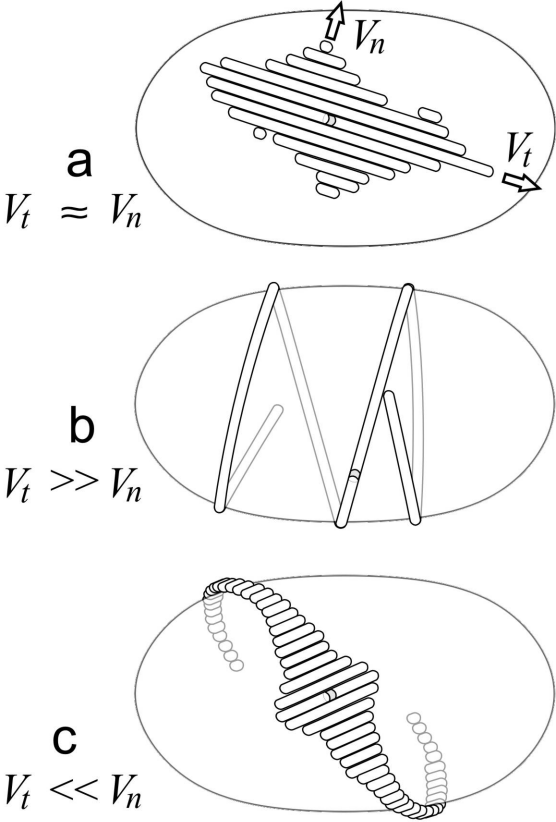

Fig. 2
Malkin

a
b
c

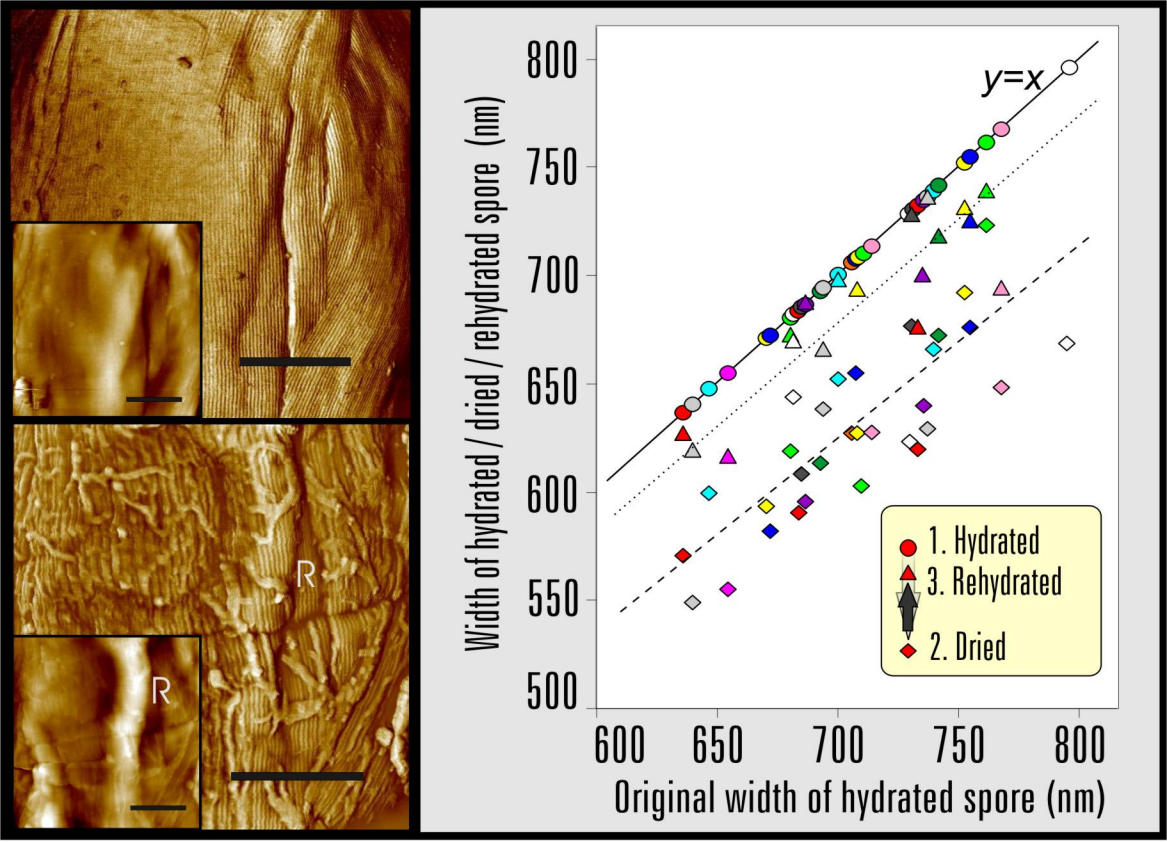

Fig. 3
Malkin

scalebars:

200 nm

a c
b

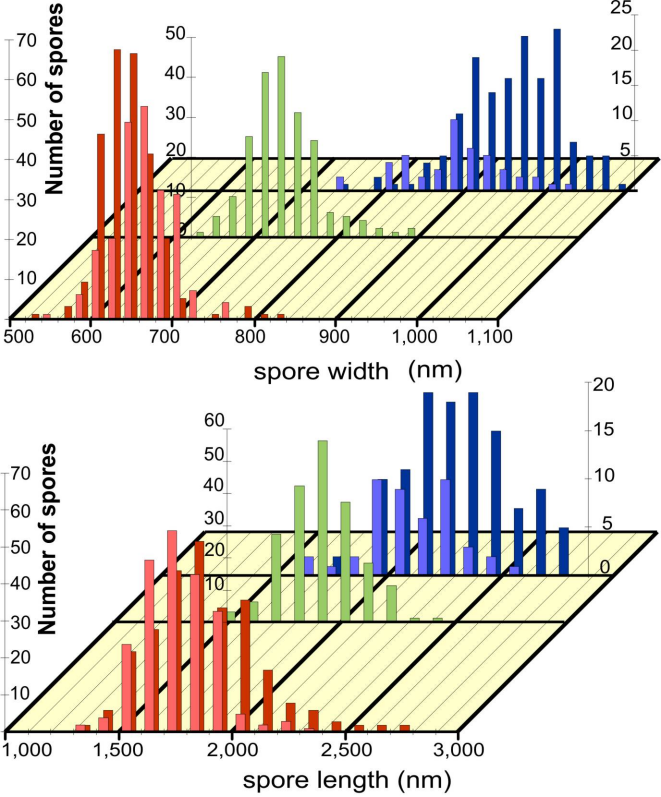

Fig. 4
Malkin

a

b